Kinetics and Mechanism of a Catalytic Chloride Ion Effect on the Dissociation of Model Siderophore Hydroxamate−Iron(III) Complexes

Hakim Boukhalfa and Alvin L. Crumbliss*

Department of Chemistry, Duke University, Box 90346, Durham, North Carolina 27708-0346

Received January 15, 2001

Proton-driven ligand dissociation kinetics in the presence of chloride, bromide, and nitrate ions have been investigated for model siderophore complexes of Fe(III) with the mono- and dihydroxamic acid ligands $R_1C(=O)N(OH)R_2$ ($R_1 = CH_3$, $R_2 = H$; $R_1 = CH_3$, $R_2 = CH_3$; $R_1 = C_6H_5$, $R_2 = H$; $R_1 = C_6H_5$, $R_2 = C_6H_5$) and $CH_3N(OH)C(=O)[CH_2]_nC(=O)N(OH)CH_3$ (H_2L^n; $n = 2, 4, 6$). Significant rate acceleration in the presence of chloride ion is observed for ligand dissociation from the bis(hydroxamate)- and mono(hydroxamate)-bound complexes. Rate acceleration was also observed in the presence of bromide and nitrate ions but to a lesser extent. A mechanism for chloride ion catalysis of ligand dissociation is proposed which involves chloride ion dependent parallel paths with transient Cl^- coordination to Fe(III). The labilizing effect of Cl^- results in an increase in microscopic rate constants on the order of 10^2-10^3. Second-order rate constants for the proton driven dissociation of dinuclear Fe(III) complexes formed with H_2L^n were found to vary with Fe−Fe distance. An analysis of these data permits us to propose a reactive intermediate of the structure $(H_2O)_4Fe(L^n)Fe(HL^n)(Cl)(OH_2)^{2+}$ for the chloride ion dependent ligand dissociation path. Environmental and biological implications of chloride ion enhancement of Fe(III)−ligand dissociation reactions are presented.

Introduction

(Hydroxamato)iron(III) complexes have been investigated in relation to the predominance of the hydroxamate binding site in siderophores.[1−7] The mechanism of ligand exchange and dissociation from the metal center has been investigated to enhance our understanding of iron bio-availability and iron−siderophore coordination chemistry.[1,6,7] Kinetic investigations have been used as a powerful tool to assess the coordination chemistry of ferrioxamine B.[8,9] At neutral pH ferrioxamine B is present in solution as a monomeric tris(hydroxamato)iron-(III) complex. For tetradentate hydroxamate ligands, complexes of multiple nuclearity and stoichiometry are formed.[10] In appropriate ligand to iron(III) ratios at neutral pH, all hydroxamate complexes adopt a tris(hydroxamate) binding mode.[11−13] The tris- to bis- to mono(hydroxamato)iron(III) complex interconversion mechanism and iron(III) release which occurs under a H^+ gradient has been described for a number of synthetic and natural siderophores.[14−18]

Ligand substitution at a metal center is known to be catalyzed by small molecules and ions.[19−21] For example, chloride ion enhancements of mono(acetohydroxamato)iron(III) and -(betaine hydroxamato)iron(III) complex formation and dissociation rate constants have been reported.[21] A significant rate increase suggests the participation of Cl^- in the inner coordination shell of Fe(III), which apparently labilizes the dissociating donor atoms, such as the hydroxamate group in the ligand dissociation process and water in the chelation step.

* Address correspondence to this author. E-mail: alc@chem.duke.edu. Fax: (919)660-1605.

(1) Albrecht-Gary, A.-M.; Crumbliss, A. L. In *Iron Transport and Storage in Microoganisms, Plants and Animals*; Vol. 35 of Metal Ions in Biological Systems; Sigel, A., Sigel, H., Eds.; M. Dekker, Inc.: New York, 1998; p 239.
(2) Raymond, K. N.; Telford, J. R. In *Bioinorganic Chemistry: An Inoganic Perspective of Life*; Kessissoglou, D. P., Ed.; NATO ASI Series C: Mathematical and Physical Science-Vol. 459; Kluwer Academic Publishers: Dordrecht, The Netherlands, 1995; p 25.
(3) Matzanke, B. F.; Müller-Matzanke, G.; Raymond, K. N. In *Iron Carriers and Iron Proteins*; Loehr, T. M., Ed.; VCH Publishers: New York, 1989; Chapter 1.
(4) Winkelmann, G., Carrano, C. J., Eds. *Transition Metals in Microbial Metabolism*; Harwood Academic Publishers: Reading, U.K., 1997.
(5) Telford, J. R.; Raymond, K. N. In *Molecular Recognition: Receptors for Cationic Guests*; Comprehensive Supramolecular Chemistry Vol. 1; Lehn, J.-M., Exec. Ed.; Gokel, G. W., Vol. Ed.; Pergamon Press: London, 1996; p 245.
(6) Albrecht-Gary, A.-M.; Crumbliss, A. L. In *Scientific Bridges for 2000 and Beyond*; Institut de France, Académie des Science, Editions TEC & DOC: Paris, 1999; p 73.
(7) Crumbliss, A. L. In *Handbook of Microbial Iron Chelates*; Winkelmann, G., Ed.; CRC Press: Boca Raton, FL, 1991; p 177.
(8) Monzyk, B.; Crumbliss, A. L. *J. Am. Chem. Soc.* **1982**, *104*, 4921.
(9) Biruš, M.; Bradić, Z.; Krzanric, G.; Kujundzić, N.; Pribanić, M.; Wilkins, P. C.; Wilkins, R. G. *Inorg. Chem.* **1987**, *26*, 1000.
(10) Spasojević, I.; Boukhalfa, H.; Stevens, R. D.; Crumbliss, A. L. *Inorg. Chem.* **2001**, *40*, 49.
(11) Carrano, C. J.; Cooper, S. R.; Raymond, K. N. *J. Am. Chem. Soc.* **1979**, *101*, 599.
(12) Carrano, C. J.; Raymond, K. N. *J. Am. Chem. Soc.* **1978**, *100*, 5371.
(13) Hou, Z.; Sunderland, C. J.; Nishio, T.; Raymond, K. N. *J. Am. Chem. Soc.* **1996**, *118*, 5148.
(14) Biruš, M.; Bradić, Z.; Kujundzić, N.; Pribanić, M.; Wilkins, P. C.; Wilkins, R. G. *Inorg. Chem.* **1985**, *24*, 3980.
(15) Caudle, M. T.; Crumbliss, A. L. *Inorg. Chem.* **1994**, *33*, 4077.
(16) Boukhalfa, H.; Crumbliss, A. L. *Inorg. Chem.* **2000**, *39*, 4318.
(17) Caudle, M. T.; Cogswell, L. P., III; Crumbliss, A. L. *Inorg. Chem.* **1994**, *33*, 4759.
(18) Boukhalfa, H.; Brickman, T. J.; Armstrong, S. K.; Crumbliss, A. L. *Inorg. Chem.* **2000**, *39*, 5591.
(19) See for example pp 213−217 in: Crumbliss, A. L. In *Handbook of Microbial Iron Chelates*; Winkelmann, G., Ed.; CRC Press: Boca Raton. FL, 1991; p 177.
(20) Biruš, M.; Bradic, Z.; Krzanric, G.; Kijundzic, N.; Pribanic, M. *Croat. Chem. Acta*. **1983**, *56*, 61.
(21) Biruš, M.; Krznaric, G.; Pribanić, M.; Ursic, S. *J. Chem. Res., Synop.* **1985**, 4.

10.1021/ic010050k CCC: $20.00
Published on Web 07/19/2001

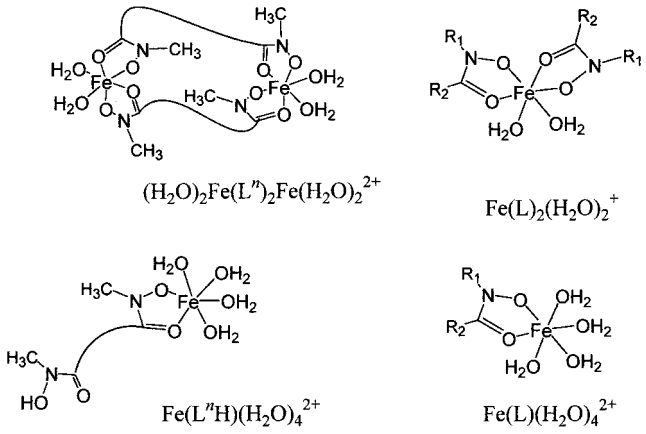

Figure 1. Structural formulas for bis- and mono(hydroxamato)−Fe(III) complexes investigated. For the mono(hydroxamic acids) $R_1C(O)N(OH)R_2$: $R_1 = CH_3$, $R_2 = H$ for L = AHA; $R_1 = R_2 = CH_3$ for L = NMAHA; $R_1 = C_6H_5$, $R_2 = H$ for L = BHA; $R_1 = C_6H_5$, $R_2 = C_6H_5$ for L = PBHA.

In this work we report a chloride, bromide, and nitrate ion effect on the ligand dissociation kinetics from tetradentate and bidentate (hydroxamato)iron(III) complexes, whose structures are shown in Figure 1. These complexes exhibit anion effects for both mononuclear and binuclear Fe(III) species. Kinetic results show a significant rate enhancement in the presence of chloride ion at relatively low concentrations. A model describing the species involved in the chloride-mediated dissociation mechanism is proposed. A chloride ion effect on the dissociation rate suggests the presence of one ($FeCl^{2+}$) or two ($FeCl_2^{+}$) chloride ions in the inner coordination shell of Fe(III). The labilizing effect of bromide and nitrate is much lower than the effect of the chloride ion. The importance of charge interactions in the dissociation process for diiron complexes will be discussed in the context of a model that considers the Coulombic interactions between the charged complex and the incoming proton.

Experimental Section

Materials. Stock solutions of 2.0 M NaCl (Mallinckrodt AR Analytical Reagent), $NaClO_4$ (Aldrich 99+%), NaBr (Aldrich 99+%), and $NaNO_3$ (Aldrich 99+%) were prepared from their solid salts in deionized water and standardized by passing through a Dowex 50 W-X8 strong acid cation-exchange column in the H^+ form. Ferric perchlorate stock solution (0.1 M) was prepared from recrystallized ferric perchlorate hydrate and standardized spectrophotometrically in strong acid[22] and titrimetrically by reduction with Sn(II) and titrating with the primary standard potassium dichromate.[23] A 2.0 M $HClO_4$ stock solution was prepared from concentrated perchloric acid (Fisher 70%) and standardized by titration with standard NaOH solution to the phenolphthalein end point. pH measurements were made using a Corning 250 pH/ion meter equipped with an Orion ROSS pH electrode filled with 3.0 M NaCl solution. The dihydroxamic acid ligands were prepared according to the method described in the literature[24] and were recrystallized and characterized as described elsewhere.[17] The mono(hydroxamic acid) ligands acetohydroxamic acid (AHA) and benzohydroxamic acid (BHA) were purchased from Aldrich (99+%) and used without any further purification. *N*-Phenylbenzohydroxamic acid was prepared and characterized as described elsewhere.[27b] The tetradentate iron(III) complexes were prepared by reacting $Fe(ClO_4)_3$ with the dihydroxamate ligand H_2L^2, H_2L^4, and H_2L^6 (H_2L^n, $[CH_3N(OH)C{=}O)]_2(CH_2)_n$, where n represents the carbon chain length between the two hydroxamate units) in 1:1 Fe(III)-to-ligand ratio and the pH was adjusted between 2.0 and 2.5. The ionic strength was kept constant at $I = 2.0$ M ($NaCl/NaClO_4$). All bis(hydroxamato)iron(III) complexes prepared exhibit a strong absorbance characteristic of two hydroxamate moieties coordinated to Fe(III) ($\lambda_{max} = 470$, $\epsilon = 1600-1800$ M^{-1} cm^{-1}/Fe).[17]

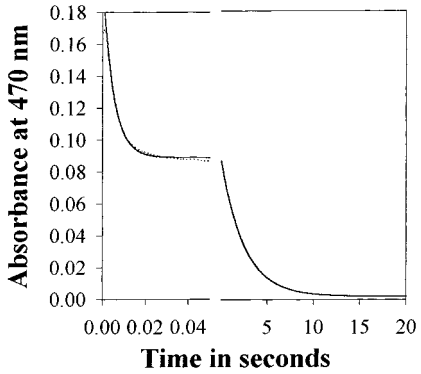

Figure 2. Time-dependent absorbance decay for the H^+ driven dissociation of the bis complex $Fe(NMAHA)_2(H_2O)_2^{+}$. The first and the second absorbance decays were recorded separately on a 50 ms and 20 s time scale, respectively. The raw data are presented as a dashed line, and the fit to the experimental data according to eq 1 is presented as a solid line. First decay: $Abs_{eq} = 0.0868$; $B = 0.1109$; $k^{obsd}_t = 200.6$ s^{-1}. Second decay: $Abs_{eq} = 0.0003$; $B = 0.08628$; $k^{obsd}_t = 0.39$ s^{-1}. Conditions: $\lambda = 470$ nm; $[Fe(NMAHA)_2(H_2O)_2^{+}] = 2 \times 10^{-3}$ M; $[H^+] = 0.5$ M; $[Cl^-] = 0.4$ M; $I = 2$ M ($NaClO_4/NaCl/HClO_4$); $T = 25$ °C.

Kinetic Measurements. Ligand dissociation kinetics were performed using an Applied Photophysics stopped-flow instrument (SX.18 MV), equipped with a diode array spectrophotometer with an approximate range of 200−750 nm. The effect of different anions on the bis(hydroxamato)iron(III) dissociation rates was examined by varying the anion and acid concentrations. All measurements were performed under pseudo-first-order conditions of excess acid and the anion under investigation, at 25 °C and constant ionic strength $I = 2.0$ (NaX, $NaClO_4/HClO_4$; $X^- = Cl^-$, Br^-, NO_3^-). Absorbance decay data were analyzed using the Applied Photophysics kinetic software.

Results

General Observations. We did not observe any rate enhancement due to anion effects for tris chelated Fe(III) complexes of the ligands investigated. This suggests the need for a labile aquated coordination site on Fe(III) for anion catalysis to be operative. This assertion will be examined in more detail below. Significant rate enhancement was observed for bis- and mono(hydroxamato)iron(III) complexes in the presence of chloride ion and, to a much lesser extent, bromide and nitrate.

The bis(hydroxamato)iron(III) complex displays a strong charge-transfer band at ca. 470 nm. Upon complex dissociation the absorbance maximum shifts to a higher wavelength (ca 500 nm). Under the proton gradient applied ($[H^+]$ from 0.1 to 1.0

(22) Bastian, R.; Weberling, R.; Padilla, F. *Anal. Chem.* **1956**, *28*, 459.
(23) Vogel. A. I. *Quantitative Inorganic Analysis Including Elementary Instrumental Analysis*, 3rd ed.; Longmans, Green and Co., Ltd.: London, 1968.
(24) (a) Hauser, C. R.; Renfrow, W. B. *Org. Synth.* **1943**, *2*, 67. (b) Caudle M. T.; Crumbliss, A. L. *Inorg. Chem.* **1994**, *33*, 4077.
(25) Boukhalfa. H.; White, P. Crumbliss, A. L. Manuscript in preparation.
(26) Barclay, S.; Huynh. H. B.; Raymond. K. N. *Inorg. Chem.* **1984**, *23*, 2011.
(27) (a) Monzyk B.; Crumbliss, A. L. *J. Am. Chem. Soc.* **1979**, *101*, 6203. (b) Brink, C. P.; Crumbliss, A. L. *Inorg. Chem.* **1984**, *23*, 4708.

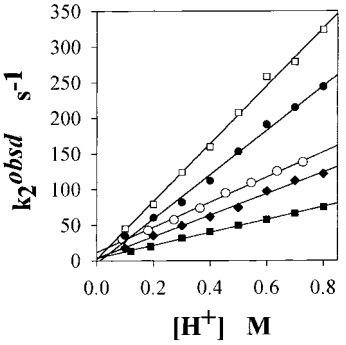

Figure 3. Kinetic data for the acid-driven dissociation of the bis complex $Fe(NMAHA)_2(H_2O)_2^+$. Conditions: $[Fe^{3+}] = 0.3$ mM; [NMAHA] = 0.6 mM; $I = 2.0$ M ($NaClO_4$/NaCl/$HClO_4$); $T = 25$ °C; initial pH = 2.31. The solid lines represent a linear regression fit to the data (Table S1) according to eq 4. Key: (■) kinetic data in the absence of chloride ion, slope = 90.5(2) M^{-1} s^{-1} and intercept = 3.39-(0.7) s^{-1}; (◆) $[Cl^-] = 0.1$ M, slope = 150.8(4) M^{-1} s^{-1} and intercept = 3.4(2) s^{-1}; (○) $[Cl^-] = 0.2$ M, slope = 176 (4) M^{-1} s^{-1} and intercept = 11.8(2) s^{-1}; (●) $[Cl^-] = 0.3$ M Cl^-, slope = 310(10) M^{-1} s^{-1} and intercept = −3(5) s^{-1}; (□) $[Cl^-] = 0.4$ M, slope = 405(10) M^{-1} s^{-1} and intercept = 2.7(5) s^{-1}.

M) the bis(hydroxamato)iron(III) complex undergoes complete-dissociation giving rise to two successive absorbance decays monitored at 470 nm (Figure 2). The apparent dissociation rate constants were obtained by analyzing the absorbance change according to eq 1, where Abs_t and Abs_{eq} are the absorbance at time t and infinite time, respectively, B is the amplitude of the absorbance change, and k^{obsd} is the apparent ligand dissociation rate constant.

$$Abs_t - Abs_{eq} = Be^{-k^{obsd}t} \quad (1)$$

In the presence of chloride ion the bis- and mono(hydroxamato)iron(III) complex dissociation rate constants are enhanced by several orders of magnitude relative to the data obtained in the presence of the noncoordinating ion ClO_4^-. While bromide and nitrate also exhibited a rate acceleration effect, it was relatively small ($Br^- > NO_3^-$) and consequently was not investigated in detail. The experiments were performed at fixed ionic strength $I = 2.0$ M ($NaClO_4$/NaX/$HClO_4$; X = Cl^-, Br^-, NO_3^-) and constant temperature $T = 25$ °C. The chloride ion effect is measured through an examination of the apparent dissociation rate constant variation with a gradual increase in Cl^- concentration. The hydroxamate ligand dissociation from the bimetallic bis(di-hydroxamate) complexes $(H_2O)_2Fe(L^n)_2Fe(H_2O)_2^{2+}$ and the monometallic bis(mono-hydroxamate) complex $Fe(NMAHA)_2(H_2O)_2^+$ (Figure 1) exhibit distinct kinetic profiles and will be presented separately.

Bis-Chelated Monometallic Complex $Fe(NMAHA)_2(H_2O)^{2+}$ Dissociation. The bis to mono complex dissociation is enhanced in the presence of chloride ion as is shown from the dependence of the apparent dissociation rate constant on Cl^- concentrations (Figure 3).

Coupled reactions 2 and 3 in Scheme 1 are proposed to describe the proton-assisted dissociation of the bis(*N*-methylacetohydroxamato)iron(III) complex in the presence of Cl^-,

Scheme 1[a]

$$Fe(L)_2^+ + H^+ \underset{k_{-2}}{\overset{k_2}{\rightleftharpoons}} Fe(L)^{2+} + HL \quad (2)$$

(2a) $Fe(L)_2^+ + Cl^- \; K_{Fe(L)_2Cl}$ (2b) $Fe(L)^{2+} + Cl^- \; K_{Fe(L)Cl}$

$$Fe(L)_2Cl + H^+ \underset{k_{-2}^{Cl}}{\overset{k_2^{Cl}}{\rightleftharpoons}} Fe(L)Cl^+ + HL \quad (3)$$

[a] L = *N*-methylacetohydroxamato; coordinated H_2O not shown for clarity.

where HL represents $CH_3C(=O)N(OH)CH_3$. The apparent dissociation rate constant k_2^{obsd} can be expressed in terms of the ligand dissociation and formation rate constants k_2, k_2^{Cl}, k_{-2}, and k_{-2}^{Cl}, respectively, and the equilibrium constants $K_{Fe(L)Cl}$ and $K_{Fe(L)_2Cl}$ by eqs 4 and 5,

$$k_2^{obsd} = \frac{(k_2 + k_2^{Cl}K_{Fe(L)_2Cl}[Cl^-])[H^+]}{(1 + K_{Fe(L)_2Cl}[Cl^-])} + C \quad (4)$$

$$C = \left(k_{-2} + \frac{k_{-2}^{Cl}K_{Fe(L)Cl}[Cl^-]}{1 + K_{Fe(L)Cl}[Cl^-]}\right)[HL] \quad (5)$$

where $[H^+]$ and $[Cl^-]$ are present in large excess over the complex and the concentration of the ligand, [HL], is assumed to be constant. Values for $k_2 = 7.64 \times 10^1$ M^{-1} s^{-1}, $k_2^{Cl} = 3.88 \times 10^4$ M^{-1} s^{-1}, and $K_{Fe(L)_2Cl} = 2.06 \times 10^{-2}$ M^{-1} were determined from a nonlinear fit of the model in eq 4 to the experimental data (Table S1 and Figure S1 of the Supporting Information). The value obtained for k_2 is in good agreement with that obtained previously for this step in the absence of Cl^- [15] (Table 1) and therefore confirms the validity of the model presented in Scheme 1.

Bimetallic Dihydroxamic Acid Complex $(H_2O)_2Fe(L^n)_2Fe(H_2O)_2^{2+}$ Dissociation. The bimetallic complex $(H_2O)_2Fe(L^n)_2Fe(H_2O)_2^{2+}$ has a doubly ligand-bridged structure with two equivalent Fe(III) centers (Figure 1).[25] The distance between the two Fe(III) centers is dependent on the length of the carbon chain separating the two binding sites. The ligand dissociation mechanism for complexes having a $(H_2O)_2Fe(L^n)_2Fe(H_2O)_2^{2+}$ structure has been reported in 2.0 M $NaClO_4$/$HClO_4$,[16,17] and the dissociation rates were found to be dependent on the distance between the two metal centers. In the presence of chloride ion the observed apparent dissociation rate constants are significantly higher than the dissociation rate constants determined in 2.0 M sodium perchlorate. The effect of chloride ion on ligand dissociation from the bimetallic complex was investigated for ligands with a carbon chain length (between the hydroxamate groups) of 2, 4, and 6 $-CH_2-$groups ($(H_2O)_2Fe(L^n)_2Fe(H_2O)_2^{2+}$, where $n = 2$, 4, 6; Figure 1).

The apparent dissociation rate constant k_3^{obsd} for ligand dissociation from $(H_2O)_2Fe(L^n)_2Fe(H_2O)_2^{2+}$ exhibits a second-order dependence with respect to H^+ in the presence of 2.0 M ClO_4^-, a noncoordinating ion. This second-order H^+ dependence is also observed in the presence of 0.2 M X^-/1.8 M ClO_4^- (X = Cl^-, Br^-, NO_3^-) as illustrated in Figure 4A for $(H_2O)_2Fe(L^2)_2Fe(H_2O)_2^{2+}$. Bromide and nitrate ions show only a small effect on the rate of ligand dissociation. Chloride ion, however, exhibits a significant effect on k_3^{obsd} as illustrated in Figure 4B for $(H_2O)_2Fe(L^2)_2Fe(H_2O)_2^{2+}$ dissociation at various Cl^- concentrations. Similar results were obtained for $(H_2O)_2Fe(L^n)_2Fe(H_2O)_2^{2+}$ ($n = 2$, 4, 6) in the presence of Cl^-, Br^-, and NO_3^- and are listed in the Supporting Information tables. These results

Table 1. Microscopic Kinetic Parameters Defined in Schemes 1−4 for the Dissociation of Bis- and Mono(hydroxamato)iron(III) Complexes in the Presence and Absence of Chloride Ion[a]

		ligand			
reaction	parameter	L^2	L^4	L^6	NMAHA
2a	$K_{Fe(L)Cl}/M^{-1}$				$2.06 \times 10^{-2}(5.44 \times 10^{-3})$
2	$k_2/M^{-1}\ s^{-1}$				76.5(7.5), 102[b]
3	$k_2^{Cl}/M^{-1}\ s^{-1}$				$3.88 \times 10^4(10^3)$
6	K_4/M^{-1}	0.60[c]	0.84[c]	0.94[c]	
7	$k_3/M^{-1}\ s^{-1}$	1.3[c]	17.79[c]	23[c]	
7a	$K_{Fe_2(L)(LH)Cl}/M^{-1}$	0.02[d]	0.02[d]	0.02[d]	
8	$k_3^{Cl}/M^{-1}\ s^{-1}$	860(30)	9750(1500)	17400(500)	
13	k'_1	0.0069[c]	0.00233[c]	0.0015[c]	0.0071[b]
14	$k_1/M^{-1}\ s^{-1}$	0.0019[c]	0.0013[c]	0.0024[c]	0.0032[b]
14a	$K_{Fe(L)Cl}/M^{-1}$	2.66[f]	2.66[f]	2.66[f]	2.66[f]
14b	K_{FeCl}/M^{-1}	4.26[e]	4.26[e]	4.26[e]	4.26[e]
15	$k_1^{Cl}K_{Fe(L)Cl}/M^{-2}\ s^{-1}$	0.218(0.01)	1.06(0.11)	0.76(0.06)	0.166(0.11)[i]
15	$k_1^{Cl}/M^{-1}\ s^{-1}$	0.082[h]	0.40[h]	0.287[h]	0.062[h,j]
15b	$K_{Fe(Cl)_2}/M^{-1}$	1.32[e]	1.32[e]	1.32[e]	1.32[e]
16	$k_1^{Cl_2}K_{Fe(L)(Cl)_2}K_{Fe(L)(Cl)}/M^{-3}\ s^{-1}$	0.170(0.02)	0.28(0.07)	1.69	3.33(0.33)[k]

[a] $I = 2.0$ ($NaClO_4$/NaCl/$HClO_4$); $T = 25$ °C. Values in parentheses represent the standard error. [b] Values from ref 15. [c] Values from ref 17. [d] The value of $K_{Fe_2(L)(HL)Cl}$ is approximated by the value determined for the complex $Fe(NMAHA)_2Cl$ ($K_{Fe(L)_2Cl}$ in reaction 2a). [e] Values from ref 28. [f] The value of $K_{Fe(L)Cl}$ is approximated by the value of $K_{Fe(AHA)Cl}$ for acetohydroxamic acid from ref 21. [g] The value of $K_{Fe(L)Cl_2}$ is approximated by the value of $K_{Fe(AHA)Cl_2}$ for acetohydroxamic acid from ref 21. [h] Values determined using the $k_1^{Cl}K_{Fe(L)Cl}$ values and the value of $K_{Fe(L)Cl_2}$ computed from values in ref 21. [i] The values for AHA, BHA, and PBHA are $k_1^{Cl}K_{Fe(L)Cl} = 16.51\ M^{-2}\ s^{-1}$, $k_1^{Cl}K_{Fe(L)Cl} = 6.65\ M^{-2}\ s^{-1}$, and $k_1^{Cl}K_{Fe(L)Cl} = 2.91\ M^{-2}\ s^{-1}$, respectively. [j] The values for k_1^{Cl} for AHA, BHA, and PBHA are $k_1^{Cl} = 6.2\ M^{-1}\ s^{-1}$, $k_1^{Cl} = 2.5\ M^{-1}\ s^{-1}$, and $k_1^{Cl} = 1.1\ M^{-1}\ s^{-1}$, respectively. [k] The values $k_1^{Cl_2}K_{Fe(L)(Cl)_2}K_{Fe(L)(Cl)}$ for AHA, BHA, and PBHA are $k_1^{Cl_2}K_{Fe(L)(Cl)_2}K_{Fe(L)(Cl)} = 31.52\ M^{-3}\ s^{-1}$, $k_1^{Cl_2}K_{Fe(L)(Cl)_2}K_{Fe(L)(Cl)} = 17.34\ M^{-3}\ s^{-1}$, and $k_1^{Cl_2}K_{Fe(L)(Cl)_2}K_{Fe(L)(Cl)} = 5.92\ M^{-3}\ s^{-1}$, respectively.

Scheme 2[a]

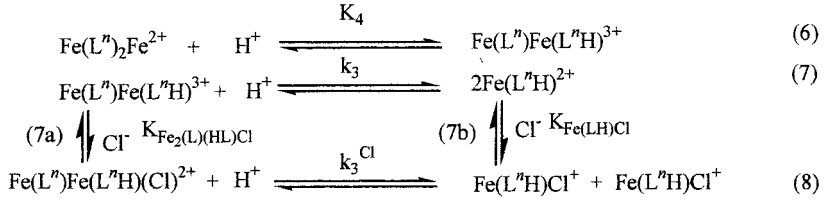

[a] H_2L^n, $n = 2, 4, 6$; coordinated H_2O omitted for clarity.

are interpreted as a parallel ligand dissociation pathway as illustrated in Scheme 2. The apparent ligand dissociation rate constant, k_3^{obsd}, is expressed by eq 9, where the microscopic rate parameters are as defined in Scheme 2. Assuming the values of $K_{Fe_2(L)(LH)Cl}$ and $K_{Fe(LH)Cl}$ are small, eq 9 simplifies to eq 10.

$$k_3^{obsd} = \frac{(k_3 + k_3^{Cl}K_{Fe_2(L)(LH)Cl}[Cl^-])K_4[H^+]^2}{1 + K_4[H^+](1 + K_{Fe_2(L)(LH)Cl}[Cl^-])} + 2\left(k_{-3} + \frac{k_{-3}K_{Fe(LH)Cl}[Cl^-]}{1 + K_{Fe(LH)Cl}[Cl^-]}\right) \quad (9)$$

$$k_3^{obsd} = \frac{(k_3 + k_3^{Cl}K_{Fe_2(L)(LH)Cl}[Cl^-])K_4[H^+]^2}{1 + K_4[H^+]} + 2(k_{-3} + k_{-3}K_{Fe(LH)Cl}[Cl^-]) \quad (10)$$

The rate constant k_3 and the preequilibrium constant K_4 were fixed to their values determined in the absence of the chloride ion from our previous investigation,[16,17] and the value of $K_{Fe_2(L)(LH)Cl}$ was fixed at $2.06 \times 10^{-2}\ M^{-1}$ as determined for chloride coordination to the complex $Fe(NMAHA)_2(H_2O)_2^+$. The ligand dissociation rate constant, k_3^{Cl}, was determined from a nonlinear fit of eq 10 to the experimental data (Table 1). Figure 4A,B presents the experimental data and the numerical fit for the proton driven dissociation of the complex $(H_2O)_2Fe(L^2)_2Fe(H_2O)_2^{2+}$. Results of the numerical fits and derived parametersfor $(H_2O)_2Fe(L^n)_2Fe(H_2O)_2^{2+}$ ($n = 2, 4, 6$) are listed in Table 1.

Mono(hydroxamate) Complex Dissociation. The mono(hydroxamato)iron(III) complexes $Fe(NMAHA)(H_2O)_4^{2+}$ and $Fe(L^nH)(H_2O)_4^{2+}$ shown in Figure 1 are characterized by their UV−vis spectra with an absorbance maximum at ca. 500 nm.[26] With an increase in the proton concentration ([H^+] from 0.1 to 1.0 M), the complexes undergo slow ligand dissociation according to proton-dependent and -independent parallel paths producing both $Fe(H_2O)_6^{3+}$ and $Fe(H_2O)_5OH^{2+}$.[27] In the presence of chloride ion the apparent dissociation rate constants for the proton dependent path are enhanced by several orders of magnitude. Figure 5 represents a plot of the apparent dissociation rate constant for a series of mono(hydroxamate)-coordinated complexes ($Fe(L)^{2+}$) as a function of the chloride ion concentration at different proton concentrations. At constant chloride ion concentration the apparent dissociation rate constant increases linearly with the proton concentration (Figure S2 in the Supporting Information). These data at fixed [Cl^-] may be described by eq 11, where the slope, b, exhibits second-order [Cl^-] dependence as described by eq 12, and illustrated in Figure 5 for various complexes $Fe(L)(H_2O)_4^{2+}$ (where L represents AHA, NMAHA, BHA, PBHA, $(HL^4)^-$, and $(HL^6)^-$). The corresponding k_1^{obsd} values are tabulated in Table S3 in the Supporoting Information.

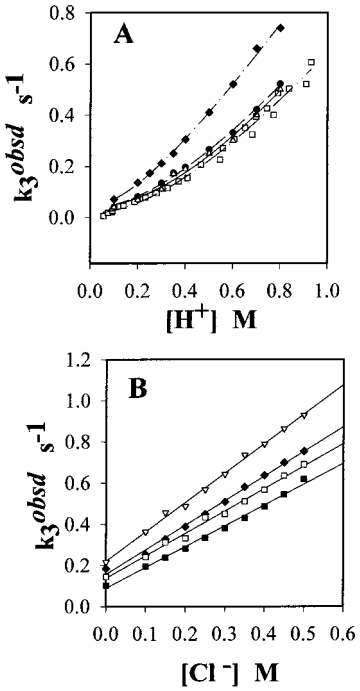

Figure 4. Kinetic data for the acid-driven dissociation of the bis complex $(H_2O)_2Fe(L^2)_2Fe(H_2O)_2^{2+}$. Conditions: $[Fe^{3+}] = 0.3$ mM; $[H_2L^2] = 0.3$ mM; $I = 2.0$ M ($NaClO_4$/NaX/$HClO_4$; X = Cl^-, Br^-, NO_3^-); $T = 25$ °C; initial pH = 2.45. (A) Plot of k_3^{obsd} as function of $[H^+]$ at constant anion concentration: (□) only ClO_4^- anion present at 2.0 M; (Δ) $[NO_3^-] = 0.2$ M, $[ClO_4^-] = 1.8$ M; (●) $[Br^-] = 0.2$ M, $[ClO_4^-] = 1.8$ M; (◆) $[Cl^-] = 0.2$ M, $[ClO_4^-] = 1.8$ M. Solid lines represent a fit of eq 10 to the data. (B) Plot of k_3^{obsd} as function of Cl^- ion concentration at $[H^+] = 0.3$ (■), 0.35 (□), 0.4 (◆), and 0.45 (▽) M, respectively. Lines represent a fit of eq 10 to the data.

$$k_1^{obsd} = a + b[H^+] \quad (11)$$

$$b = c + d[Cl^-] + e[Cl^-]^2 \quad (12)$$

A model for $Fe(L)(H_2O)_4^{2+}$ (L = AHA, NMAHA, BHA, PBHA$^-$, and HL^{n-}) complex dechelation is presented in Scheme 3, which describes parallel hydroxamic acid ligand dissociation paths involving the product species $Fe(H_2O)_6^{3+}$, $Fe(H_2O)_5OH^{2+}$, $Fe(H_2O)_5Cl^{2+}$, and $Fe(H_2O)_4(Cl)_2^+$. By consideration of this scheme as a relaxation process, the dissociation of the mono complex $Fe(L)(H_2O)_4^{2+}$ in Scheme 3 can be described by eq 17,

Scheme 3[a]

$$Fe(L)^{2+} + H_2O \underset{}{\overset{k'_1/k'_{-1}}{\rightleftharpoons}} Fe(OH)^{2+} + HL \quad (13)$$

$$K_h \Updownarrow H^+$$

$$Fe(L)^{2+} + H^+ \overset{k_1/k_{-1}}{\rightleftharpoons} Fe^{3+} + HL \quad (14)$$

$$(14a) \Updownarrow Cl^- K_{Fe(L)Cl} \qquad \Updownarrow Cl^- K_{Fe(Cl)} \quad (14b)$$

$$Fe(L)Cl^+ + H^+ \overset{k_1^{Cl}/k_{-1}^{Cl}}{\rightleftharpoons} Fe(Cl)^{2+} + HL \quad (15)$$

$$(15a) \Updownarrow Cl^- K_{Fe(L)Cl_2} \qquad \Updownarrow Cl^- K_{Fe(Cl)_2} \quad (15b)$$

$$Fe(L)(Cl)_2 + H^+ \overset{k_1^{Cl_2}/k_{-1}^{Cl_2}}{\rightleftharpoons} Fe(Cl)_2^+ + HL \quad (16)$$

[a] $Fe(L)^{2+}$ represents $Fe(NMAHA)(H_2O)_4^{2+}$, $Fe(AHA)(H_2O)_4^{2+}$, $Fe(BHA)(H_2O)_4^{2+}$, $Fe(PBHA)(H_2O)_4^{2+}$, and $Fe(HL^n)(H_2O)_4^{2+}$ ($n = 2$, 4, and 6).

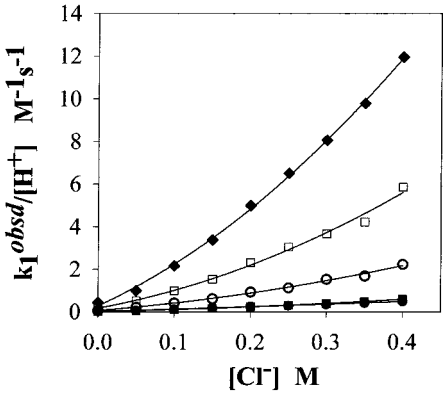

Figure 5. Plot of the apparent dissociation rate constant $k_1^{obsd}/[H^+]$ for the dissociation of the mono complex $Fe(L)^+$ (where L represents AHA (acetohydroxamic acid), BHA (benzohydroxamic acid), PBHA (N-phenylbenzohydroxamic acid), and H_2L^4 and H_2L^6 (see Figure 1)) as a function of proton and chloride ion concentrations. Conditions: $[Fe^{3+}] = 0.3$ mM; [L] = 0.6 mM; $I = 2.0$ M ($NaClO_4$/NaCl/$HClO_4$); $T = 25$ °C; initial pH = 2.31. Solid lines represent a nonlinear regression fit of eq 19 to the data: (◆) (AHA) $k_1^{Cl}K_{Fe(L)Cl} = 16.51(1.38)$ M^{-2} s^{-1}, $k_1^{Cl_2}K_{Fe(L)Cl}K_{Fe(L)Cl_2} = 31.52(3.33)$ M^{-3} s^{-1}; (□) (BHA) $k_1^{Cl}K_{Fe(L)Cl} = 6.65(1.97)$ M^{-2} s^{-1}, $k_1^{Cl_2}K_{Fe(L)Cl}K_{Fe(L)Cl_2} = 17.34(5)$ M^{-3} s^{-1}; (○) (PBHA) $k_1^{Cl}K_{Fe(L)Cl} = 2.91(0.6)$ M^{-2} s^{-1}, $k_1^{Cl_2}K_{Fe(L)Cl}K_{Fe(L)Cl_2} = 5.92(1.5)$ M^{-3} s^{-1}; (■) (H_2L^4) $k_1^{Cl}K_{Fe(L)Cl} = 1.06(0.11)$ M^{-2} s^{-1}, $k_1^{Cl_2}K_{Fe(L)Cl}K_{Fe(L)Cl_2} = 0.28(0.27)$ M^{-3} s^{-1}; (●) (H_2L^6) $k_1^{Cl}K_{Fe(L)Cl} = 0.76(0.06)$ M^{-2} s^{-1}, $k_1^{Cl_2}K_{Fe(L)Cl}K_{Fe(L)Cl_2} = 1.69(0.14)$ M^{-3} s^{-1}. Values in parentheses represent the standard error deviation.

$$k_1^{obsd} = \frac{\left(k_1 + k'_1\frac{1}{[H^+]} + k_1^{Cl}K_{Fe(L)Cl}[Cl^-] + k_1^{Cl_2}K_{Fe(L)Cl}K_{Fe(L)(Cl)_2}[Cl^-]^2\right)[H^+]}{1 + K_{Fe(L)Cl}[Cl^-] + K_{Fe(L)Cl}K_{Fe(L)Cl_2}[Cl^-]^2} + C \quad (17)$$

where

$$C = \frac{\left(k_{-1} + k'_{-1}\frac{K_h}{[H^+]} + k_{-1}^{Cl}K_{FeCl}[Cl^-] + k_{-1}^{Cl_2}K_{Fe(Cl)_2}[Cl^-]^2\right)[HL]}{1 + \frac{K_h}{[H^+]} + K_{Fe(Cl)}[Cl^-] + K_{Fe(Cl)}K_{Fe(Cl)_2}[Cl^-]^2} \quad (18)$$

Equation 17 is further simplified to eq 19 since $K_{Fe(L)Cl}$ and $K_{Fe(L)(Cl)_2}$ are small and the denominator in the first term of eq 17 is approximately 1.

$$k_1^{obsd} = \left(k_1 + k'_1\frac{1}{[H^+]} + k_1^{Cl}K_{Fe(L)Cl}[Cl^-] + k_1^{Cl_2}K_{Fe(L)Cl}K_{Fe(L)(Cl)_2}[Cl^-]^2\right)[H^+] + \text{constant} \quad (19)$$

Equation 19 is consistent with our experimental observations described by eq 11 and 12 where

$$a = k'_1 + \text{constant} \quad (20)$$

and

$$b = k_1 + k_1^{Cl}K_{Fe(L)Cl}[Cl^-] + k_1^{Cl_2}K_{Fe(L)Cl}K_{Fe(L)(Cl)_2}[Cl^-]^2 \quad (21)$$

Values for $k_1^{Cl}K_{Fe(L)Cl}$ and $k_1^{Cl_2}K_{Fe(L)Cl}K_{Fe(L)(Cl)_2}$ in Table 1 were determined for the mono(hydroxamato)iron(III) complexes with

ligands H_2L^n ($n = 2$, 4, and 6) and NMAHA by fitting eq 19 to the data using k_1 and k_1' values from previous studies[15,17] in the absence of Cl^-. The values for AHA, BHA, and PBHA for $k_1^{Cl}K_{Fe(L)Cl}$ and $k_1^{Cl_2}K_{Fe(L)Cl}K_{Fe(L)(Cl)_2}$ are included as footnotes *i* and *k* in Table 1. By assuming that $K_{Fe(L)Cl} = 2.66\ M^{-1}$, as was calculated from previously reported values,[21] the values for k_1^{Cl} were obtained (Table 1).

Discussion

Ions such as Cl^-, Br^-, and NO_3^- did not enhance ligand dissociation rates from tris(hydroxamato)iron(III) complexes but did enhance ligand dissociation from the corresponding bis and mono complexes. This suggests the necessity for these rate accelerating anions to replace one or more coordinated H_2O ligands in the inner coordination shell of the Fe(III) for their influence to be felt. The bromide and nitrate ions had a small effect on the dissociation rate constants, and we were not able to accurately quantify the rate enhancement due to the presence in solution of these two ions. However, it is clear that the dissociation reaction in the presence of these two ions is faster than in the presence of perchlorate (Figure 4A). The labilization effect in the presence of anions decreases, as follows: $Cl^- \gg Br^- > NO_3^-$. This relative order is consistent with the relative affinity of these ions for coordination to Fe(III).[28]

The linear correlation between the bis complex dissociation rate constants and the chloride ion concentration for both $Fe(NMAHA)_2(H_2O)_2^+$ and $(H_2O)_2Fe(L^n)_2Fe(H_2O)_2^{2+}$ suggests the introduction of one chloride ion in the inner coordination sphere of Fe(III) prior to hydroxamate ligand dissociation. This Cl^- effect results in a 500−750-fold rate enhancement (compare the ratios k_2^{Cl}/k_2 and k_3^{Cl}/k_3 in Table 1). For the bimetallic doubly bridged complex, $(H_2O)_2Fe(L^n)_2Fe(H_2O)_2^{2+}$, ligand dissociation proceeds via a fast protonation preequilibrium reaction followed by parallel ligand dissociation reactions (Scheme 2). The dissociation of the $(H_2O)_2Fe(L^n)_2Fe(H_2O)_2^{2+}$ complex is controlled by the rate at which the intermediates $(H_2O)_4Fe(L^n)Fe(HL^n)(H_2O)_2^{3+}$ and $(H_2O)_4Fe(L^n)Fe(HL^n)(H_2O)(Cl)^{2+}$ undergo ligand dissociation. The dissociation rate enhancement is due to the introduction of the chloride ion into the inner coordination sphere of Fe(III), which increases the lability of the other ligands resulting in a faster ligand exchange reaction. This result is in good agreement with literature results for the significant increase in the water exchange rate from $Fe(H_2O)_6^{3+}$ ($k_{H_2O} = 1.6 \times 10^2\ s^{-1}$) upon the introduction of OH^- in the Fe(III) inner coordination sphere, $Fe(H_2O)_5(OH)^{2+}$ ($k_{OH} = 1.2 \times 10^5\ s^{-1}$).[29] The increase in the water exchange rate by a factor of 750 is attributed to the electron-donating ability of the hydroxide ion relative to water. By formation of a strong Fe−OH bond, the interaction between the iron center and the remaining water ligands is weakened, which results in faster ligand exchange.

The rate acceleration effect of Cl^- on the ligand dissociation process for the bimetallic bis-coordinated complexes is also illustrated in Figure 6. The ligand dissociation rate constant for the bimetallic complexes $(H_2O)_2Fe(L^n)_2Fe(H_2O)_2^{2+}$ is influenced by the distance between the two Fe(III) centers and the dielectric constant of the medium,[16,17] both in the presence and absence of Cl^- ion. This result is interpreted according to a model described below that is based on an electrostatic repulsion between the incoming proton and the positively charged complex.

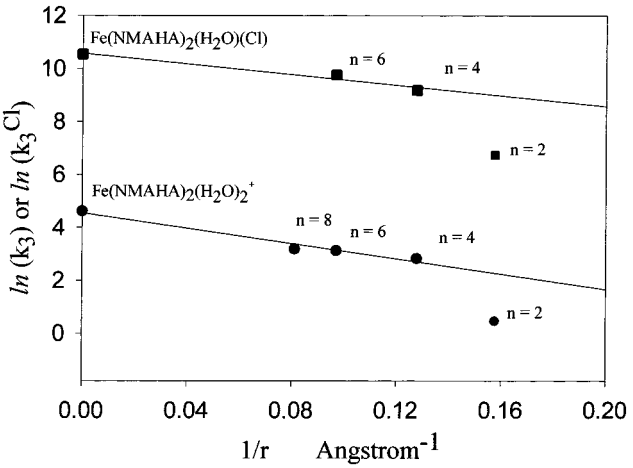

Figure 6. Effect of the Fe−Fe distance on the dissociation rate constants for ligand dissociation from $(H_2O)_2Fe(L^n)_2Fe(H_2O)_2^{2+}$ complexes. *n* represents the carbon chain length between the two hydroxamate units. Key: (●) data in 2.0 M $NaClO_4$ from refs 15 and 16; (■) data in 2.0 M $NaCl/NaClO_4$ in the presence of chloride ion. The plot represents the logarithm of the rate constant for reaction 7 (●, k_3) or reaction 8 (■, k_3^{Cl}) plotted as a function of the reciprocal of the Fe−Fe distance in the complex. The Fe−Fe distance was estimated from molecular mechanics conformational studies[15] normalized for the Fe−Fe distance in $(H_2O)_2Fe(L^2)Fe(H_2O)_2^{2+}$ determined from single-crystal X-ray diffraction.[25] A linear fit of eq 25 to the data excluding the data point for $n = 2$ gave a slope of −14.4 and intercept 4.47, $R^2 = 0.97$, for ● and a slope of −10.03 and intercept 10.5, $R^2 = 0.96$, for ■.

Let us assume that the free energy of activation for the ligand dissociation process in reaction 8 of Scheme 2 ($\Delta G^*_3{}^{Cl}$) can be described as the sum of two components (eq 22),

$$\Delta G^*_3{}^{Cl} = \Delta G^*_{int} + \Delta G^*_{elec} \qquad (22)$$

one which represents an intrinsic barrier to proton-assisted hydroxamate ligand dissociation (ΔG^*_{int}) and another which represents the electrostatic repulsion which the incoming proton experiences from the neighboring Fe(III) center as it attacks the Fe(III) center undergoing ligand dissociation (ΔG^*_{elec}). Scheme 4 is an expansion of reactions 7 and 8 shown in Scheme 2 which illustrates the two possible sites of attack for Cl^-, Fe_A and Fe_B. In Scheme 4 we show a preequilibrium step prior to reaction 8 (reaction 7a′ or 7a″) which involves a single Cl^- ion entering the inner coordination shell of Fe(III). Reaction 7a in Scheme 2 may involve substitution of Cl^- for H_2O at either Fe_A or Fe_B but not both, since the kinetics of hydroxamate ligand dissociation in reaction 8 are first order in [Cl^-]. The location of the Cl^- in the inner coordination shell of Fe_A or Fe_B alters the electrostatic contribution to $\Delta G^*_3{}^{Cl}$. Since H^+ attack at $(H_2O)_4Fe_A(L^n)Fe_B(HL^n)(H_2O)(Cl)^{2+}$ (Scheme 4, structure **4-3**) or $(H_2O)_3(Cl)Fe_A(L^n)Fe_B(HL^n)(H_2O)_2^{2+}$ (Scheme 4, structure **4-2**) must occur at Fe_B in order to yield a mono(hydroxamato)-iron(III) complex product in reaction 8, the two possibilities for this process may be envisioned as follows. The electrostatic contribution to the energy barrier $\Delta G^*_3{}^{Cl}$ for path 8′ in Scheme 4 leads to eq 23[16,17]

$$\Delta E = (2+)(1+)e^2(1/\epsilon r) - (1+)(1+)e^2(1/\epsilon r) = e^2/\epsilon r \qquad (23)$$

where *e* is the fundamental unit of electrostatic charge (4.8×10^{-10} esu), ϵ is the dielectric shielding constant at the reaction center, *r* is the distance between Fe_A and Fe_B in angstroms, and ΔE is the electrostatic repulsion that the incoming proton experiences from the net 1+ charged Fe_A center as it approaches

(28) Smith, R. M.; Martell, A. E. *Critical Stability Constants*; Plenum Publ Co.: New York, 1976; Vol. 4, pp 50, 106, 116.
(29) Swaddle, T. W.; Merbach, A. E. *Inorg. Chem.* **1981**, *20*, 4212.

Scheme 4

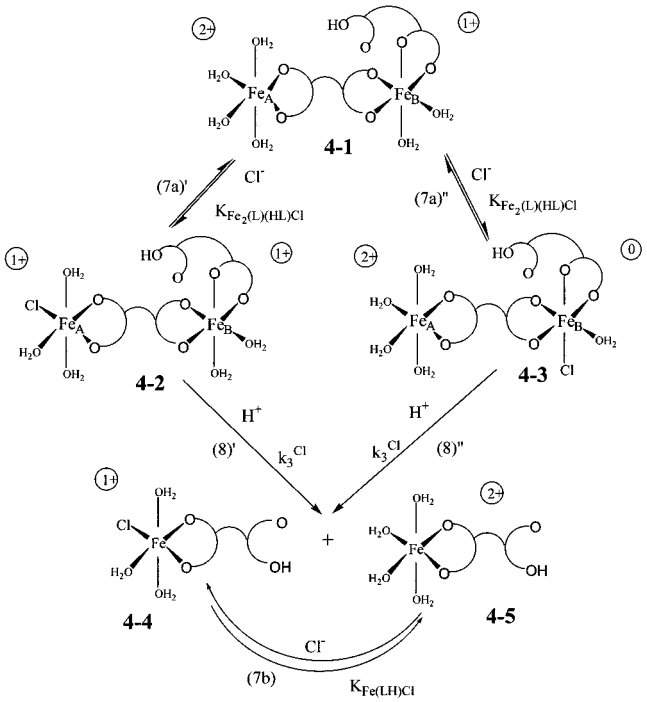

the 1+ charged Fe_B center. The electrostatic contribution to the energy barrier $\Delta G^*_3{}^{Cl}$ for path 8″ is different, as the attacking proton experiences a repulsion from a net 2+ charged Fe_A center as it approaches an uncharged Fe_B center. This case is described by eq 24.

$$\Delta E = (2+)(1+)e^2(1/\epsilon r) - (2+)(0+)e^2(1/\epsilon r) = 2e^2/\epsilon r \quad (24)$$

Equation 23 or 24 can be used with eq 22 to develop an equation for $k_3{}^{Cl}$ [16,17]

$$\ln k_3{}^{Cl} = -S(1/\epsilon r) + \ln k_{3(int)}{}^{Cl} \quad (25)$$

where $S = 0.55 \times 10^3$ when path 8′ (Scheme 4) is operative and eq 23 is used and $S = 1.1 \times 10^3$ when path 8″ is operative and eq 24 is used. Equation 25 predicts a linear plot of $\ln(k_3{}^{Cl})$ vs $1/r$ as illustrated in Figure 6. This plot shows that as the distance between Fe_A and Fe_B decreases, the proton-driven ligand dissociation process becomes slower. The intercept is consistent with the second-order rate constant $k_2{}^{Cl}$ for ligand dissociation from $Fe(NMAHA)_2(H_2O)(Cl)^+$, which represents the intrinsic ligand dissociation reaction barrier when the second Fe(III) center is an infinite distance away from the Fe(III) reaction center.

An important observation to be made in Figure 6 is that the two lines describing the variation in the uncatalyzed and catalyzed rate constants k_3 and $k_3{}^{Cl}$ with Fe_A-Fe_B distance are *approximately parallel*, i.e., have the same slope. This is consistent with the formation of $(H_2O)_4Fe_A(L^n)Fe_B(HL^n)(OH_2)Cl^{2+}$ (species **4-3** in Scheme 4) in reaction 7a″ and *not* the alternative structure, **4-2**. This conclusion is based on two facts. The first is that in the uncatalyzed reaction the electrostatic contribution to the reaction barrier is described by eq 26[16,17]

$$\Delta E = (2+)(2+)e^2(1/\epsilon r) - (2+)(1+)e^2(1/\epsilon r) = 2e^2/\epsilon r \quad (26)$$

which produces the same $2e^2/\epsilon r$ result as eq 24. This means that in eq 25 $S = 1.1 \times 10^3$ for the uncatalyzed reaction. Furthermore, it means that whatever value is used for the shielding dielectric constant ϵ in the uncatalyzed and catalyzed cases, the slopes of plots of $\ln k_3{}^{Cl}$ vs $1/r$ and $\ln k_3$ vs $1/r$ will be equivalent if path (8″) is operative in the Cl^- catalyzed case. The slope for the Cl^--catalyzed reaction would be expected to be 0.5 that of the uncatalyzed reaction if path (7a′)−(8′) in Scheme 4 were operative. The second fact is that the labilizing effect of the Cl^- donor is more likely to be felt when it is in the inner coordination shell of the reactive Fe site (Fe_B) rather than the neighboring site (Fe_A), as is the case with structure **4-3**, $(H_2O)_4Fe_A(L^n)Fe_B(HL^n)(OH_2)Cl^{2+}$.

From eq 25 it is evident that the slope in Figure 6 is related to the effective dielectric constant (ϵ) at the reaction site. If the $n = 2$ data point is ignored for both the uncatalyzed and Cl^--catalyzed system, the dielectric constant at the reactive site calculated from the slope in Figure 6 is ca. 80, effectively that of bulk water. The negative deviation of the $n = 2$ data point for both the Cl^--catalyzed and uncatalyzed dissociation of $(H_2O)_4Fe(L^2)Fe(HL^2)(H_2O)_2{}^{3+}$ suggests a lower reactive site dielectric constant (ca. 50), consistent with a shorter Fe−Fe distance and the concomitant diminished access of bulk solvent to the reactive site. We do not wish to emphasize the quantitative aspects of this argument, but it is consistent with the electrostatic model used to analyze the trends in the data in Figure 6. Further discussion of this point is found in ref 16.

The increase in the intercept in Figure 6 attributed to the intrinsic dissociation rate is in good agreement with the labilizing effect exhibited by the chloride ion. The chloride ion is a more effective electron pair donor than H_2O, which decreases the energy barrier for hydroxamate ligand dissociation and thereby increases the intrinsic dissociation rate constant.

We are unable to extract values for the microscopic rate constants $k_1{}^{Cl}$ and $k_1{}^{Cl_2}$ in Scheme 3 for the acid-dependent ligand dissociation from $Fe(L)Cl^+$ and $Fe(L)Cl_2$, respectively. However, by assuming $K_{Fe(L)Cl} = 2.66\ M^{-1}$ for reaction 14a obtained from the analogous reaction of Cl^- with $Fe(AHA)(H_2O)_4{}^{2+}$,[21] the ratio $k_1{}^{Cl}/k_1$ is approximated as 50 for the dihydroxamate H_2L^n ligand and 20 for NMAHA (Table 1). Our results are in full agreement with the literature[21] for chloride ion enhancement of the acid-driven dissociation of acetohydroxamic acid from $Fe(AHA)(H_2O)_4{}^{2+}$; we find the ratio $k_1{}^{Cl}/k_1 = 100$ and $k_1{}^{Cl} = 6.2\ M^{-1}\ s^{-1}$ ($k_1{}^{Cl} = 6.0\ M^{-1}\ s^{-1}$ [21]).

The rate-limiting step in the formation and dissociation of (hydroxamato)iron(III) complexes has been attributed to the formation and cleavage of the Fe−carbonyl bond, respectively; ring closure and opening is considered to be fast.[27] Ligand dissociation proceeds according to parallel paths producing $Fe(H_2O)_5(OH)^{2+}$ and $Fe(H_2O)_6{}^{3+}$ (reactions 13 and 14 in Scheme 3).[27] In the absence of a coordinating anion such as Cl^-, the path involving the species $Fe(H_2O)_5(OH)^{2+}$ has been found to be faster in both formation and dissociation directions. The enhancement in the rate is related to the activation mechanism and the *labilizing* effect of coordinated OH^-. The path involving the species $Fe(H_2O)_5(OH)^{2+}$ proceeds through a dissociative-interchange mechanism (I_d), and the path involving the species $Fe(H_2O)_6{}^{3+}$ proceeds according to an associative-interchange mechanism (I_a).

In the presence of Cl^-, we do not observe an acid-independent ligand dissociation path (Figure S2 in the Supporting Information and Scheme 3). This is likely due to the fact that, with Cl^- in the inner coordination shell, the remaining H_2O ligands will exhibit diminished Brønsted acidity. This effect is expected to increase the coordinated water pK_a for both $Fe(L)(H_2O)_3Cl^+$ (relative to $FeL(H_2O)_4{}^{2+}$) and $Fe(H_2O)_5Cl^{2+}$ (relative to $Fe(H_2O)_6{}^{3+}$). Consequently, Cl^- ion catalysis of the acid-

independent ligand dissociation path (or its reverse; reaction 13 in Scheme 3) is not observed.

Conclusions

We conclude that chloride ion accelerates the kinetics of hydroxamate ligand dissociation from mononuclear and dinuclear Fe(III) complexes which have a labile coordinated H_2O that can be substituted by a Cl^-. The labilizing effect is approximately a factor of 10^2-10^3, which is commensurate with the rate acceleration of H_2O ligand exchange caused by the presence of OH^- in the inner coordination shell. Our mechanistic study is enhanced by an evaluation of the correlation of ligand dissocation rate constants from a dinuclear Fe(III) complex with Fe−Fe distance, which enables us to propose that the reactive intermediate has the structure $(H_2O)_4Fe(L^n)Fe(HL^n)(H_2O)(Cl)^{2+}$. Since the hydroxamic acid ligands investigated here serve as models for siderophores, the labilizing effect of a Cl^--containing medium has environmental and biological implications. High environmental Cl^- concentrations, or intracellular compartments with enhanced Cl^- concentrations, will certainly enhance the release of siderophore-bound Fe(III).

Acknowledgment. We gratefully acknowledge financial support from the NSF.

Supporting Information Available: Figures showing the influence of H^+ and Cl^- on the rate of ligand dissociation from $Fe(NMAHA)_2(H_2O)_2^+$ and $Fe(NMAHA)(H_2O)_4^{2+}$ and tables of observed rate constants at various H^+ and Cl^- concentrations for hydroxamate ligand dissociation from all of the mono- and dihydroxamic acid complexes of Fe(III) reported here. This material is available free of charge via the Internet at http://pubs.acs.org.

IC010050K